

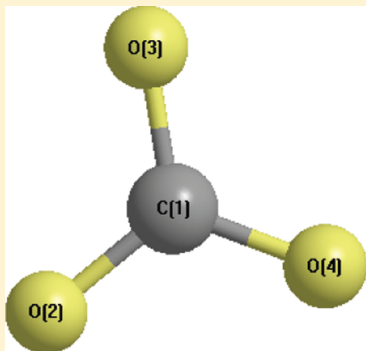
DFT Models of Molecular Species in Carbonate Molten Salts

W. Robert Carper,*† Phillip G. Wahlbeck,† and Trevor R. Griffiths‡

†Department of Chemistry, Wichita State University, Wichita, Kansas 67260-0051, United States

‡Redston Trevor Consulting Ltd., 58 High Ash Avenue, Leeds LS17 8RF, U.K.

ABSTRACT: Raman spectra of high temperature carbonate melts are correlated with carbonate species modeled at 923 K using B3LYP/(6-311+G(2d,p)) density functional calculations. Species that are theoretically stable at 923 K include O^{2-} , O_2^- , O_2^{2-} , CO_3^{2-} , $C_2O_6^{2-}$, CO_4^- , CO_4^{2-} , CO_4^{4-} , CO_5^{2-} , KCO_4^- , $LiCO_4^-$, KO_2^- , LiO_2^- , NaO_2^- , KO_2 , LiO_2 , NaO_2 , KCO_3^- , $LiCO_3^-$, and $NaCO_3^-$. Triangular, linear, and bent forms are theoretically possible for KO_2^- and NaO_2^- . Triangular and linear forms may exist for LiO_2^- . Linear and triangular versions are theoretically possible for LiO_2^- and KO_2 . A triangular version of NaO_2 may exist. The correlation between measured and theoretical Raman spectra indicate that monovalent cations are to be included in several of the species that produce Raman spectra.



INTRODUCTION

Molten carbonate research plays an important role in several areas that include the development of efficient fuel cells,^{1–10} spent nuclear fuel degradation,^{11,12} and nerve gas oxidation.¹³ Research developments in these seemingly unrelated areas are dependent on the correct identification of various carbonate related species that exist in carbonate melts.

In particular, molten carbonate fuel cell (MCFC) technology is a rapidly growing area of energy research. Molten carbonate fuel cells have the ability to reach fuel conversion to electricity efficiencies of 50% and thermal efficiencies of greater than 80%.^{7–10} As molten carbonate fuel cells are being developed, the identification of active species in molten carbonates becomes critical. Raman spectroscopy has been used in recent years to identify possible species found in molten carbonates.^{1–6} The advantage of using Raman spectra rather than IR spectra is due to the complexity of overlapping bands in IR spectra that are difficult to deconvolute. Assignments of Raman absorption bands have been made by a number of investigators.^{1–6} Although these assignments appear to be reasonable, they lack detailed theoretical support of the type that has proved useful in similar studies of ionic liquids.^{14–16} In recent years, investigators have used ab initio calculations and Raman spectra to probe both the overall and local structures of ionic liquids as outlined in detail in several excellent reviews.^{17,18}

In this study, a number of theoretically stable oxygen-containing species including carbonates have been modeled. The calculated Raman spectra are seen to match the reported Raman spectra with a high degree of accuracy. Previously ignored carbonate and oxygen-containing species are identified as major contributors to the Raman spectral bands.

METHODS

Computational Methods. The density functional theory (DFT) calculations were obtained using Gaussian 03 in a tight

fit configuration.¹⁹ The B3LYP (6-311+(2d,p)) level of computation was used for all structures. Calculated vibrational frequencies of the various structures contain no imaginary frequencies, ensuring the presence of a minimum. The eigenvectors for each normal mode were displayed on the computer and the normal modes were assigned to specific group vibrations in a manner similar to previous vibrational frequency studies of ionic liquids.^{14–16}

Frequency Correlations. The correlations between calculated and experimental spectra are based primarily on Raman peak intensities and frequencies (cm^{-1}).^{14–16} This approach avoids the IR problem in cases where adjacent experimental frequencies overlap and require deconvolution.

Molecular Structures. The calculated gas phase structures include the following: O^{2-} , O_2^- , O_2^{2-} , CO_3^{2-} , $C_2O_6^{2-}$, CO_4^- , CO_4^{2-} , CO_4^{4-} , CO_5^{2-} , KCO_4^- , $LiCO_4^-$, KO_2^- (three versions), LiO_2^- (two versions), NaO_2^- (three versions), KO_2 (two versions), LiO_2 (two versions), NaO_2 , KCO_3^- , $LiCO_3^-$, and $NaCO_3^-$. These and other related structures were determined at the B3LYP/(6-311+G(2d,p)) level of computation. DFT theory is usually quite successful in predicting accurate molecular structure and vibrational frequencies.^{17,18}

RESULTS AND DISCUSSION

Gas Phase Structures. Figures 1–25 contain the DFT structures determined at the B3LYP/(6-311+G(d,p)) level of computation. The linear structures of CO_2 , O_2 , O_2^- , and O_2^{2-} are not shown for the sake of brevity.

The possible existence of a number of these species is somewhat unexpected. In addition to the usual planar form of CO_3^{2-} (Figure 1), a stable planar form of CO_3^- (Figure 2) may

Received: February 20, 2012

Revised: April 11, 2012

Published: April 18, 2012

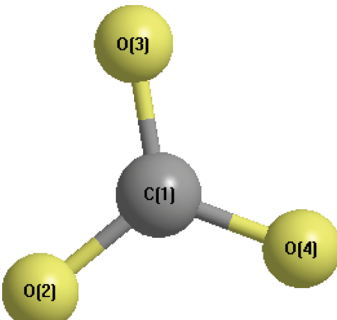


Figure 1. Planar CO_3^{2-} . All C–O distances = 1.306 Å.

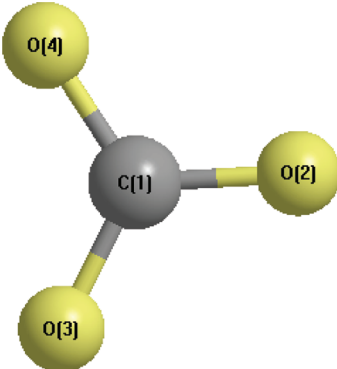


Figure 2. Planar CO_3^- . All C–O distances = 1.270 Å.

also exist. Tetrahedral structures of CO_4^{2-} , CO_4^{2-} , and CO_4^{4-} (Figures 3, 6, and 9) have been determined as were structures

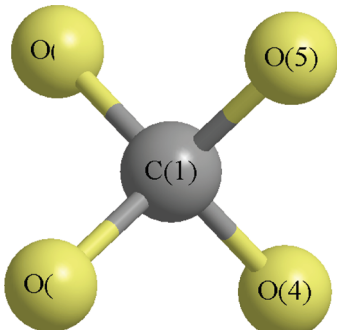


Figure 3. Tetrahedral CO_4^{2-} . All C–O distances = 1.375 Å.

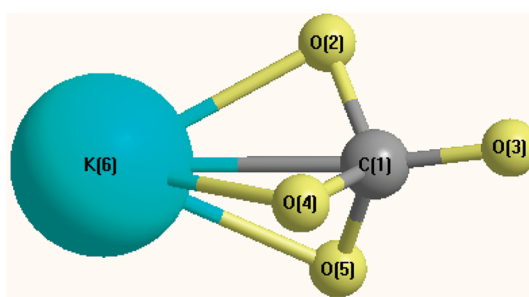


Figure 4. KCO_4^- . Bond lengths: $\text{K}-\text{C}1 = 2.630 \text{ \AA}$; $\text{K}-\text{O}2 = \text{K}-\text{O}4 = 2.456 \text{ \AA}$; $\text{K}-\text{O}5 = 2.517 \text{ \AA}$; $\text{C}1-\text{O}2 = \text{C}1-\text{O}4 = 1.388 \text{ \AA}$; $\text{C}1-\text{O}3 = 1.330 \text{ \AA}$; $\text{C}1-\text{O}5 = 1.393 \text{ \AA}$. Bond angles: $\text{K}-\text{O}4-\text{C}1 = \text{K}-\text{O}2-\text{C}1 = 81.2^\circ$; $\text{K}-\text{O}5-\text{C}1 = 78.8^\circ$; $\text{O}4-\text{C}1-\text{O}5 = 102.7^\circ$; $\text{O}5-\text{C}1-\text{O}3 = 118.7^\circ$; $\text{O}4-\text{C}1-\text{O}2 = 114.9^\circ$; $\text{O}3-\text{C}1-\text{O}2 = 109.0^\circ$; $\text{O}4-\text{C}1-\text{O}5 = 102.7^\circ$.

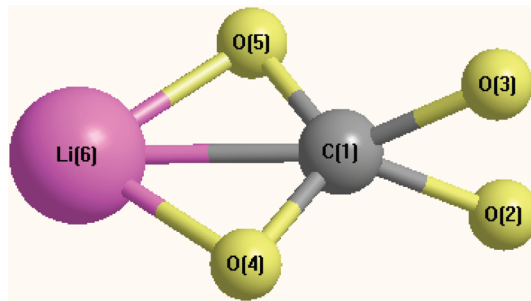


Figure 5. LiCO_4^- . Bond lengths: $\text{Li}-\text{C}1 = 2.028 \text{ \AA}$; $\text{Li}-\text{O}5 = \text{Li}-\text{O}4 = 1.741 \text{ \AA}$; $\text{C}1-\text{O}5 = \text{C}1-\text{O}4 = 1.333 \text{ \AA}$; $\text{C}1-\text{O}2 = \text{C}1-\text{O}3 = 1.450 \text{ \AA}$. Bond angles: $\text{O}5-\text{Li}-\text{O}4 = 81.1^\circ$; $\text{O}5-\text{C}1-\text{O}4 = 116.1^\circ$; $\text{O}5-\text{C}1-\text{O}3 = \text{O}2-\text{C}1-\text{O}4 = 116.8^\circ$; $\text{O}3-\text{C}1-\text{O}2 = 63.1^\circ$.

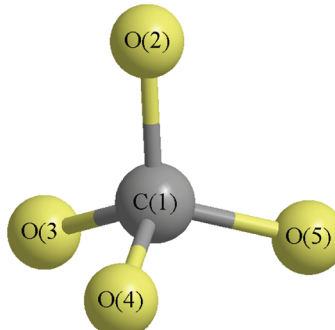


Figure 6. Tetrahedral CO_4^{4-} . All C–O distances = 1.487 Å.

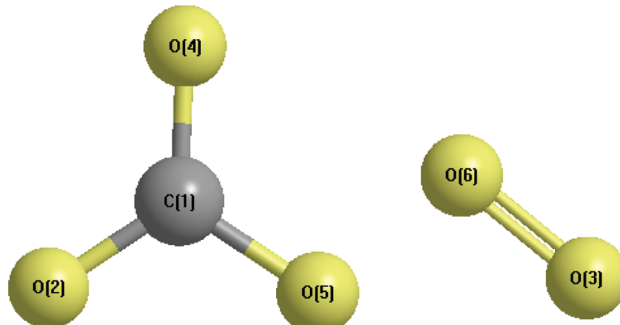


Figure 7. CO_5^{2-} . Carbonate–oxygen adduct. $\text{C}1-\text{O}2 = 1.277 \text{ \AA}$; $\text{C}1-\text{O}4 = 1.260 \text{ \AA}$; $\text{C}1-\text{O}5 = 1.351 \text{ \AA}$; $\text{O}5\cdots\text{O}6 = 1.912 \text{ \AA}$; $\text{O}6-\text{O}3 = 1.315 \text{ \AA}$. Both molecules lie in the same plane.

of an adduct of CO_3^{2-} and O_2 (Figure 7) and a dimer of CO_3^- (Figure 8). The structures of KCO_4^- and LiCO_4^- are also shown (Figures 4 and 5) and will be discussed under the section Effect of CO_2 . A potential dimer of CO_3^{2-} is theoretically unstable.

Cation Dependences. The monovalent cations, K^+ , Li^+ , and Na^+ form stable adducts with CO_3^{2-} as expected (Figures 10–12). K^+ and Na^+ interact with two of the carbonate oxygens, whereas Li^+ interacts with a single oxygen (Figure 11). The highest occupied molecular orbitals (HOMOs) of these singly charged anions are shown in Figure 13.

The theoretical peroxide structures containing K^+ , Li^+ , or Na^+ are shown in Figures 14–21. There are triangular and linear forms for KO_2^- , LiO_2^- , and NaO_2^- (Figures 14–19). There are also bent forms for KO_2^- and LiO_2^- (Figures 20 and 21). Triangular and linear forms for KO_2 and LiO_2 are also possible (Figures 22–25).

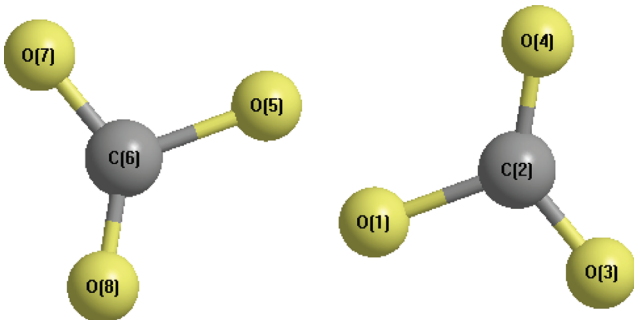


Figure 8. $(\text{CO}_3^{2-})_2$. Bond lengths: $\text{C}_6-\text{O}5 = \text{C}_2-\text{O}1 = 1.442 \text{ \AA}$; $\text{C}_6-\text{O}7 = \text{C}_2-\text{O}3 = 1.249 \text{ \AA}$; $\text{C}_6-\text{O}8 = \text{C}_2-\text{O}4 = 1.235 \text{ \AA}$; $\text{O}5\cdots\text{O}1 = 1.482 \text{ \AA}$. This dimer is slightly off-planar as shown below.

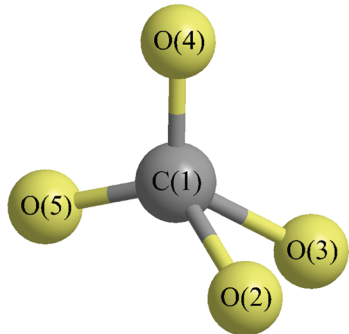


Figure 9. Distorted tetrahedral CO_4^{2-} . Bond lengths: $\text{C}_1-\text{O}4 = \text{C}_1-\text{O}5 = 1.299 \text{ \AA}$; $\text{C}_1-\text{O}2 = \text{C}_1-\text{O}3 = 1.442 \text{ \AA}$. Bond angles: $\text{O}2-\text{C}_1-\text{O}3 = 63.9^\circ$; $\text{O}2-\text{C}_1-\text{O}4 = \text{O}2-\text{C}_1-\text{O}5 = \text{O}3-\text{C}_1-\text{O}4 = \text{O}3-\text{C}_1-\text{O}5 = 120.1^\circ$; $\text{O}4-\text{C}_1-\text{O}5 = 107.7^\circ$.

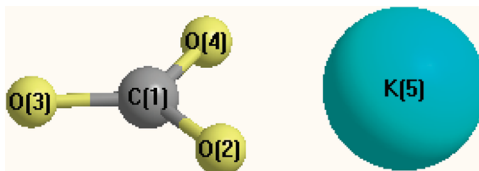


Figure 10. Planar KCO_3^{2-} . Bond lengths: $\text{C}_1-\text{O}4 = \text{C}_1-\text{O}2 = 1.299 \text{ \AA}$; $\text{C}_1-\text{O}3 = 1.300 \text{ \AA}$. Other distances: $\text{C}_1-\text{K}5 = 2.748 \text{ \AA}$; $\text{K}5-\text{O}2 = \text{K}5-\text{O}4 = 2.337 \text{ \AA}$. Bond angles: $\text{O}4-\text{C}_1-\text{O}3 = \text{O}3-\text{C}_1-\text{O}2 = 121.9^\circ$; $\text{O}4-\text{C}_1-\text{O}2 = 116.3^\circ$.

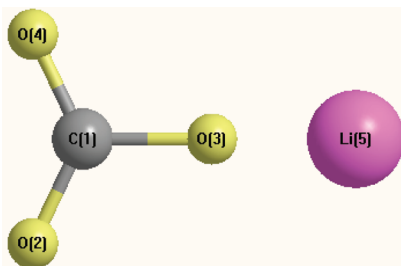


Figure 11. Planar LiCO_3^{2-} . Bond lengths: $\text{C}_1-\text{O}4 = \text{C}_1-\text{O}2 = 1.252 \text{ \AA}$; $\text{C}_1-\text{O}3 = 1.403 \text{ \AA}$. Other distances: $\text{O}3-\text{Li}5 = 1.561 \text{ \AA}$. Bond angles: $\text{O}4-\text{C}_1-\text{O}3 = \text{O}3-\text{C}_1-\text{O}2 = 115.5^\circ$; $\text{O}4-\text{C}_1-\text{O}2 = 129.1^\circ$.

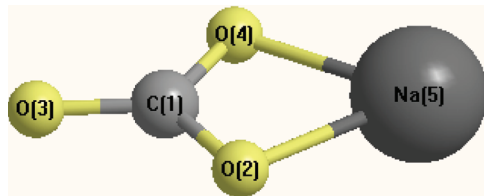


Figure 12. Planar NaCO_3^{2-} . Bond lengths: $\text{C}_1-\text{O}4 = \text{C}_1-\text{O}2 = 1.337 \text{ \AA}$; $\text{C}_1-\text{O}3 = 1.245 \text{ \AA}$; $\text{C}_1-\text{Na}5 = 2.447 \text{ \AA}$. Other distances: $\text{O}4-\text{Na}5 = \text{O}2-\text{Na}5 = 2.085 \text{ \AA}$. Bond angles: $\text{O}4-\text{C}_1-\text{O}3 = \text{O}3-\text{C}_1-\text{O}2 = 121.6^\circ$; $\text{O}4-\text{C}_1-\text{O}2 = 116.8^\circ$.

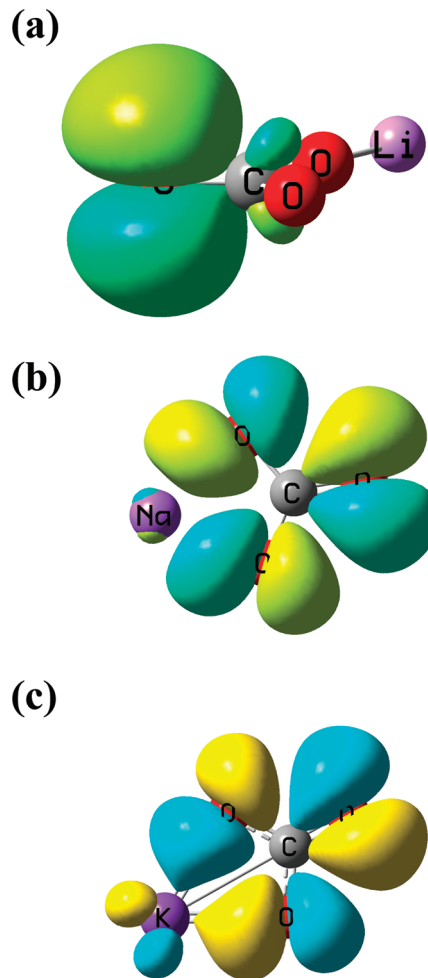


Figure 13. B3LYP/(6-311+G(2d,p)) HOMOs of (a) LiCO_3^{2-} , (b) NaCO_3^{2-} , and (c) KCO_3^{2-} .

Absolute Energies. The B3LYP/(6-311+G(2d,p)) sum of electronic and thermal free energies (au's) of potential and known species at 923 K are shown in Table 2. There is no experimental evidence for certain of these species, despite their inclusion in Table 2. However, future investigations may change this conclusion.

Peroxide Structures. Of particular interest are the various structures of peroxide containing complex anions. The bent structure of KO_2^- is the lowest energy form by 5.8 and 10.5 kcal in energy lower than the linear and triangular structures of KO_2^- at 923 K (Figures 21, 17, and 14). The triangular form of LiO_2^- is 45 kcal lower in energy than the linear form of LiO_2^- (Figures 15 and 18). The triangular and bent forms of NaO_2^-



Figure 14. B3LYP/(6-311+G(2d,p)) of KO_2^- . Bond lengths: $\text{K}-\text{O}1 = \text{K}-\text{O}2 = 2.43 \text{ \AA}$; $\text{O}2-\text{O}1 = 1.38 \text{ \AA}$. Bond angles: $\text{K}-\text{O}2-\text{O}1 = 73.6^\circ$; $\text{K}-\text{O}1-\text{O}2 = 73.3^\circ$; $\text{O}2-\text{K}-\text{O}1 = 39.1^\circ$.

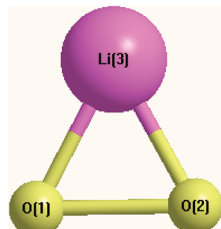


Figure 15. B3LYP/(6-311+G(2d,p)) of LiO_2^- . Bond lengths: $\text{Li}-\text{O}1 = \text{Li}-\text{O}2 = 1.67 \text{ \AA}$; $\text{O}2-\text{O}1 = 1.57 \text{ \AA}$. Bond angles: $\text{Li}-\text{O}2-\text{O}1 = \text{Li}-\text{O}1-\text{O}2 = 61.8^\circ$; $\text{O}2-\text{Li}-\text{O}1 = 56.4^\circ$.



Figure 16. B3LYP/(6-311+G(2d,p)) of NaO_2^- . Bond lengths: $\text{Na}-\text{O}1 = 2.13 \text{ \AA}$; $\text{Na}-\text{O}2 = 2.18 \text{ \AA}$; $\text{O}2-\text{O}1 = 1.41 \text{ \AA}$. Bond angles: $\text{Li}-\text{O}2-\text{O}1 = 69.2^\circ$; $\text{Li}-\text{O}1-\text{O}2 = 72.7^\circ$; $\text{O}2-\text{Li}-\text{O}1 = 38.1^\circ$.

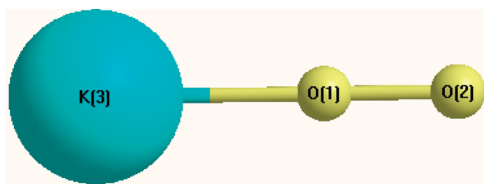


Figure 17. B3LYP/(6-311+G(2d,p)) of linear KO_2^- . Bond lengths: $\text{K}-\text{O}1 = 2.29 \text{ \AA}$; $\text{O}1-\text{O}2 = 1.34 \text{ \AA}$.

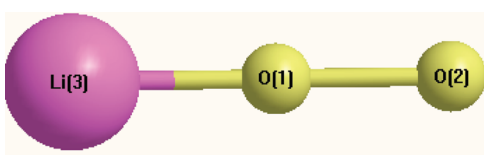


Figure 18. B3LYP/(6-311+G(2d,p)) of linear LiO_2^- . Bond lengths: $\text{Li}-\text{O}1 = 1.59 \text{ \AA}$; $\text{O}1-\text{O}2 = 1.36 \text{ \AA}$.

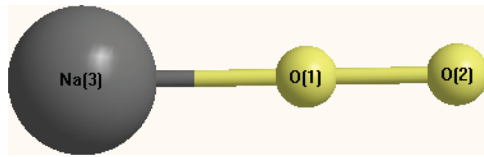


Figure 19. B3LYP/(6-311+G(2d,p)) of linear NaO_2^- . Bond lengths: $\text{Na}-\text{O}1 = 1.99 \text{ \AA}$; $\text{O}1-\text{O}2 = 1.34 \text{ \AA}$.

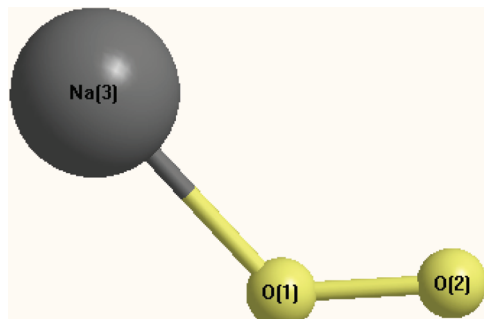


Figure 20. B3LYP/(6-311+G(2d,p)) of bent NaO_2^- . Bond lengths: $\text{Na}-\text{O}1 = 2.16 \text{ \AA}$; $\text{O}1-\text{O}2 = 1.34 \text{ \AA}$. Bond angle: $\text{Na}-\text{O}1-\text{O}2 = 129.3^\circ$.

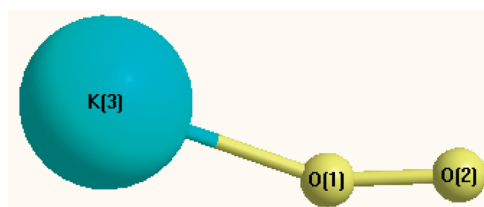


Figure 21. B3LYP/(6-311+G(2d,p)) of bent KO_2^- . Bond lengths: $\text{K}-\text{O}1 = 2.37 \text{ \AA}$; $\text{O}1-\text{O}2 = 1.33 \text{ \AA}$. Bond angle: $\text{K}-\text{O}1-\text{O}2 = 158.5^\circ$.

are lower in energy than the linear form by approximately 25 kcal at 923 K (Figures 16, 19, and 20).

There are single versions of KCO_3^- , LiCO_3^- , and NaCO_3^- at 923 K (Figures 10–12). Potentially stable forms of CO_4^{2-} , CO_4^{4-} , and CO_4^- are shown in Figures 3, 6, and 9. A dimer of CO_3^{2-} ($\text{C}_2\text{O}_6^{2-}$) may exist (Figure 8) as does an adduct of CO_3^{2-} and O_2 (CO_5^{2-}) (Figure 7).

Assignment of Raman Bands. The assignments in this section are made on the same basis as those reported in previous Raman analysis of ionic liquids.^{14–16} The calculated Raman frequencies were seen to match the experimental results to within 6%, as shown in Figure 26.^{14–16} This approach rules out several anions (including free carbonate) that are not coordinated to an individual monovalent cation in the high temperature carbonate melts. Species other than carbonate are also seen to require coordination by a monovalent cation.

Boyd and co-workers¹ reported the Raman spectrum of pure molten Li_2CO_3 at 492 K and reported a strong polarized band at 1072 cm^{-1} . This is assigned to the C–O–Li symmetric stretch vibration of LiCO_3^- at 1124 cm^{-1} (Table 1). A weaker band observed at 1752 cm^{-1} is assigned to the O–C–O in-plane asymmetric stretch at 1806 cm^{-1} in Table 1. In a separate article, Itoh and co-workers³ reported the spectrum of Li_2CO_3 at 1123 K in an O_2/CO_2 (90/10) atmosphere. They observed Raman bands at 613, 805, and 1065 cm^{-1} . The Raman band at 1065 cm^{-1} (not observed by Boyd et al.¹) is tentatively assigned to the C–O–Li symmetric stretch band at 1124 cm^{-1} with a possible contribution at 1081 cm^{-1} from the higher energy



Figure 22. B3LYP/(6-311+G(2d,p)) of triangular KO_2 . Bond lengths: $\text{K}-\text{O}1 = \text{K}-\text{O}2 = 2.39 \text{ \AA}$; $\text{O}1-\text{O}2 = 1.34 \text{ \AA}$. Bond angles: $\text{K}-\text{O}1-\text{O}2 = \text{K}-\text{O}2-\text{O}1 = 73.7^\circ$; $\text{O}2-\text{K}-\text{O}1 = 32.6^\circ$.



Figure 23. B3LYP/(6-311+G(2d,p)) of triangular LiO_2 . Bond lengths: $\text{Li}-\text{O}1 = \text{Li}-\text{O}2 = 1.75 \text{ \AA}$; $\text{O}1-\text{O}2 = 1.36 \text{ \AA}$. Bond angles: $\text{Li}-\text{O}1-\text{O}2 = \text{Li}-\text{O}2-\text{O}1 = 67.3^\circ$; $\text{O}2-\text{Li}-\text{O}1 = 45.3^\circ$.

linear forms of LiO_2^- (Table 1). The Raman frequency at 805 cm^{-1} is assigned to the triangular KO_2^- O-K-O symmetric bend frequency at 804 cm^{-1} as discussed under

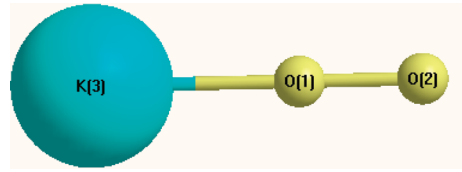


Figure 24. B3LYP/(6-311+G(2d,p)) of linear KO_2^- . Bond lengths: $\text{K}-\text{O}1 = 2.23 \text{ \AA}$; $\text{O}1-\text{O}2 = 1.32 \text{ \AA}$.

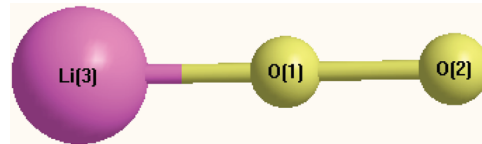


Figure 25. B3LYP/(6-311+G(2d,p)) of linear LiO_2^- . Bond lengths: $\text{Li}-\text{O}1 = 1.61 \text{ \AA}$; $\text{O}1-\text{O}2 = 1.31 \text{ \AA}$.

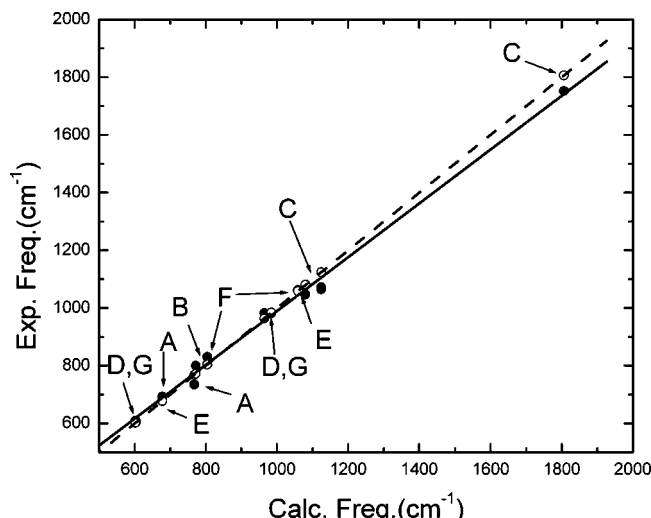
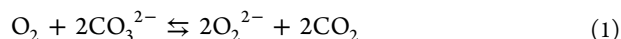


Figure 26. Experimental frequency (cm^{-1}) vs calculated frequency (cm^{-1}) for molten carbonate species: A, LiO_2^- ; B, KO_2^- ; C, LiCO_3^- ; D, CO_4^{2-} ; E, KCO_3^- ; F, LiO_2^- ; G, CO_4^{2-} , KCO_4^- . Dashed line (theoretical correlation) = slope = 1.00; solid line slope = 0.94 ($R = 0.997$).

the section Peroxides. The assignment of the Raman band at 613 cm^{-1} is assigned in the peroxide section that follows.

Peroxides. Lin and co-workers² report a series of experiments in which molten Li/K eutectic carbonate solutions in the presence of either O_2 or Ar were subjected to a wide range of temperatures. When O_2 is present, one observes a sharp peak at 1062 cm^{-1} and a weaker broad peak at 830 cm^{-1} . The Raman peak at 830 cm^{-1} is absent in the presence of Ar, and the peak at 1062 cm^{-1} shifts to 1058 cm^{-1} . The authors assign the 830 cm^{-1} band to peroxide produced via eq 1:



The above gas phase reaction, eq 1, is quite endothermic ($\Delta G^\circ = +218 \text{ kcal/mol}$); however, when K^+ ions are added to form KO_2^- , the overall process becomes exothermic ($\Delta G^\circ \approx -202$ to -207 kcal/mol ; see Table 2). The addition of Li^+ ions to form LiO_2^- is even more exothermic ($\Delta G^\circ = -261$ to -284 kcal/mol ; see Table 2). In view of the above, the broad band at 830 cm^{-1} is assigned to the strong theoretical band at 804 cm^{-1} for the triangular version of KO_2^- in Table 1. This assignment is made even though the triangular form of KO_2^- is

Table 1. B3LYP/(6-311+G(d,p)) Vibrational Assignments (cm^{-1})

species	assignment	Raman int	polarization	IR int	species	assignment	Raman int	polarization	IR int
CO_3^{2-}	K—O—C bend	137.28	0.01 p	<0.01	8	K—O—C sym bend	602.13	0.09 p	0.02
	O—C—O wag	670.72	0.21 p	<0.01	9	O—C—O sym str	888.41	0.44 dp	0.02
	O—C—O sym bend	670.72	0.21 p	<0.01	10	O—C—O asym str	938.94	0.95 p	0.99
	O—C—O out-of-plane sym bend	890.94	none	0.03	11	O—C—O asym str	943.65	1.00 dp	0.74
	O—C—O sym str	1015.99	1.00 dp	none	12	O—C—O asym str	1121.87	0.49 dp	0.11
	O—C—O in-plane asym str	1424.66	0.08 p	1.00	LiCO_4^-	1 Li—O—C bend	159.58	0.03 p	0.08
	O—C—O in-plane asym str	1425.17	0.08 p	1.00		2 O—C—O bend	380.7	0.02 p	none
	CO ₃ —O ₂ bend	73.48	0.01 p	<0.01		3 O—C—O bend	424.32	0.41 p	0.02
	CO ₃ —O ₂ bend	117.35	<0.01 p	<0.01		4 O—Li—O bend	507.51	0.01 p	0.01
	CO ₃ —O ₂ bend	129.89	0.08 dp	<0.01		5 Li—O—C sym str	543.98	0.14 dp	0.09
	CO ₃ —O ₂ bend	172.22	0.46 dp	0.03		6 Li—O—C asym str	660.8	0.17 p	0.02
	CO ₃ —O ₂ bend, O—C—O asym bend	422.07	0.03 dp	0.08		7 Li—O—C sym str	779.26	0.69 dp	0.12
CO_5^{2-}	CO ₃ —O ₂ bend, O—C—O asym bend	657.87	0.10 dp	0.01		8 O—C—O asym bend and str	784.64	1.00 p	0.06
	CO ₃ —O ₂ bend, O—C—O asym bend	702.46	0.10 dp	0.02		9 Li—O sym str	833.28	0.75 dp	0.04
	O—C—O out-of-plane asym bend	848.6	<0.01 p	0.03		10 O—C—O sym str	968.27	0.32 dp	<0.01
	O—C—O in-plane asym str	981.04	0.31 dp	0.06		11 O—C—O asym str	1221.85	0.02 p	0.90
	O—C—O in-plane asym str, O—O sym str	1159.16	0.05 dp	1.00		12 Li—C—O sym str	1232.84	0.51 dp	1.00
	O—C—O in-plane asym str, O—O sym str	1316.86	1.00 dp	0.48	CO_4^{4-}	1 O—C—O wag	439.38	0.25 p	<0.01
	O—C—O in-plane asym str, O—O sym str	1591.85	0.13 dp	0.63		2 O—C—O wag	439.44	0.25 p	<0.01
	O—C—O asym bend and str	375.13	0.03 p	0.99		3 O—C—O asym str	443.27	0.59 p	0.29
	O—C—O asym bend and str	375.75	0.03 p	0.99		4 O—C—O asym str	443.42	0.59 p	0.29
	O—C—O out-of-plane sym bend and str	842.57	none	1.00		5 O—C—O asym str	443.64	0.59 p	0.29
	O—C—O sym str	1100.14	0.27 dp	none		6 O—C—O sym str	654.26	1.00 p	none
CO_3^-	O—C—O asym str	1289.49	1.00 p	0.04		7 O—C—O asym str	938.51	<0.01 p	1.00
	O—C—O asym str	1289.64	1.00 p	0.04		8 O—C—O asym str	938.74	<0.01 p	1.00
	O—C—O wag	358.09	0.25 p	none	O_2^{2-}	9 O—C—O asym str	938.96	<0.01 p	1.00
	O—C—O asym str	428.05	0.18 p	0.04		1 O—O str	642	1.00 dp	none
	O—C—O sym bend	508.34	0.60 dp	<0.01		2 CO ₃ ⁻ —CO ₃ ⁻ bend	9.63	<0.01 dp	<0.01
	O—C—O asym bend	524.22	0.2 p	<0.01		3 CO ₃ ⁻ —CO ₃ ⁻ bend	81.86	<0.01 dp	<0.01
	O—C—O asym bend and str	745.7	<0.01 p	0.12		4 CO ₃ ⁻ —CO ₃ ⁻ bend	144.83	0.02 p	<0.01
	O—C—O asym bend and str	775.11	0.78 dp	0.06		5 CO ₃ ⁻ —CO ₃ ⁻ bend	236.47	<0.01 p	<0.01
	O—C—O sym str	987.01	1.00 dp	0.03		6 O—C—O asym bend, O—C—O asym str	263.66	0.10 dp	<0.01
	O—C—O asym str	1125.28	0.35 p	0.02		7 O—C—O asym bend, O—C—O asym str	425.34	0.12 dp	<0.01
	O—C—O asym str	1355.24	0.63 dp	1.00		8 O—C—O asym bend, O—C—O asym str	623.37	<0.01 p	0.02
CO_4^-	O—C—O wag	282.03	0.62 p	none		9 O—C—O asym bend, O—C—O sym str	637.9	<0.01 p	0.01
	O—C—O wag	378.17	0.30 dp	none		10 O—C—O out-of-plane sym bend	726.35	0.46 dp	<0.01
	O—C—O wag	402.75	0.47 p	1.00		11 O—C—O out-of-plane sym bend	808.25	0.01 dp	0.05
	O—C—O wag	402.75	0.47 p	1.00	$(\text{CO}_3^-)_2$	12 C—O in-plane sym str	812.63	<0.01 p	<0.01
	O—C—O bend and str	603.01	0.62 p	0.04		13 C—O in-plane asym str	844.09	<0.01 p	0.60
	O—C—O sym str	904.56	1.00 dp	none		14 C—O in-plane asym str and bend	862.02	1.00 dp	<0.01
	O—C—O asym str	1018.65	0.79 p	0.54		15 O—C—O in-plane sym str	934.34	0.15 dp	<0.01
	O—C—O asym str	1018.65	0.79 p	0.54		16 O—C—O in-plane sym str	1273.75	<0.01 p	0.95
	O—C—O asym str	1036.67	0.49 p	0.79		17 O—C—O in-plane asym str	1331.46	0.37 dp	0.01
	O—C—O bend	442.09	0.23 dp	0.32		18 O—C—O in-plane asym str	1765.82	<0.01 p	1.00
KCO_4^-	K—O—C bend	137.28	0.01 p	<0.01		19 O—C—O in-plane asym str	1774.48	0.06 dp	0.02
	K—O—C bend	156.11	0.01 dp	0.08	LiCO_3^-	20 C—O—Li bend	90.7	<0.01 p	0.04
	K—O str	296.38	0.15 p	0.01		21 C—O—Li bend	139.19	0.06 p	0.02
	K—O—C bend	299.66	0.39 dp	1.00		22 C—O—Li sym str, O—C—O bend	573.18	<0.01 p	<0.01
	K—O asym str	372.38	0.09 p	0.51		23 C—O—Li asym bend and str	651.19	0.07 p	0.01
	O—C—O bend	373.28	0.29 dp	0.02		24 C—O—Li sym str, O—C—O sym bend	826.45	0.22 dp	0.05
	O—C—O bend	442.09	0.23 dp	0.32		25 C—O—Li sym str, O—C—O sym bend			

Table 1. continued

species	assignment	Raman int	polarization	IR int	species	assignment	Raman int	polarization	IR int
KCO_3^-	6 C—O—Li asym str, O—C—O asym bend	845.11	<0.01 p	0.01	LiO_2^- , linear form	1 Li—O—O bend	293.93	<0.01 p	0.01
	7 C—O—Li sym str	1124.14	0.45 dp	0.13		2 Li—O—O bend	293.93	<0.01 p	0.01
	8 O—C—O in-plane sym str	1276.24	0.28 dp	0.24		3 Li—O—O sym str	771.85	0.03 dp	0.13
	9 O—C—O in-plane asym str	1805.63	1.00 p	1.00		4 Li—O—O asym str	1081.12	1.00 dp	1.00
	1 K-carbonate out-of-plane bend	67.54	<0.01 p	0.01	KO_2^- , triangular form	1 O—K—O asym str	328.85	0.02 p	0.01
	2 K-carbonate in-plane bend	266.73	<0.01 p	0.02		2 O—K—O sym str	381.03	0.20 dp	<0.01
	3 K-carbonate in-plane str	324.83	0.22 dp	0.09		3 O—K—O sym bend	803.98	1.00 dp	1.00
	4 O—C—O in-plane asym bend	615.01	0.15 p	0.01	KO_2^- , bent form	1 O—K—O asym str	95.25	0.03 dp	<0.01
	5 O—C—O in-plane sym bend	678.07	0.37 dp	0.01		2 O—K—O sym str	252.47	0.01 p	<0.01
NaCO_3^-	6 C out-of-plane inversion	852.08	0.01 p	0.01		3 O—K—O sym bend	1126.03	1.00 dp	1.00
	7 O—C—O in-plane sym str	994.25	0.26 dp	0.05	KO_2^- , linear form	1 K—O—O bend	142.72	0.04 p	0.06
	8 O—C—O in-plane asym str	1058.77	1.00 p	0.14		2 K—O—O bend	142.72	0.04 p	0.06
	9 O—C—O in-plane sym str	1577.42	0.98 dp	1.00		3 K—O str	306.64	0.04 dp	<0.01
	1 Na—carbonate out-of-plane bend	104.42	<0.01 p	0.03		4 K—O—O asym str	1080.29	1.00 dp	1.00
	2 Na—O asym str	358.4	0.03 p	<0.01	LiO_2 , triangular form	1 O—Li—O asym str	539.17	0.09 p	0.25
	3 Na—O sym str	399.51	0.03 dp	0.06		2 O—Li—O sym str	768.32	1.00 dp	1.00
	4 O—C—O wag, Na—O asym str	639.26	0.35 p	0.03		3 O—O sym str	1174.79	0.67 dp	0.08
NaO_2^- , triangular form	5 O—C—O wag, Na—O sym str	709.21	0.05 dp	<0.01	LiO_2 , linear form	1 Li—O—O bend	125.92	<0.01 p	0.34
	6 O—C—O out-of-plane bend	846.77	0.02 p	0.01		2 Li—O—O asym str	177.28	0.03 p	0.36
	7 O—C—O sym str	977.93	0.02 dp	0.04		3 Li—O—O sym str	775.35	0.08 dp	1.00
NaO_2^- , linear form	8 O—C—O asym str	1086.42	1.00 p	1.00		4 Li—O—O asym str	1323.94	1.00 dp	0.17
	9 O—C—O sym str	1584.13	0.18 dp	0.57	NaO_2 , triangular form	1 Na—O—O asym str	368.49	1.00 p	0.04
	1 Na—O—O bend	267.59	0.02 dp	0.01		2 Na—O—O sym str	436.32	0.92 dp	1.00
NaO_2^- , angular form	2 Na—O str	371.47	0.09 dp	0.05		3 O—O sym str	1167.71	0.60 dp	0.02
	3 O—O str	918.84	1.00 dp	1.00	KO_2 , triangular form	1 O—K—O asym str	332.39	0.03 p	0.08
	1 Na—O—O bend	151.57	<0.01 p	0.13		2 O—K—O sym str	353.69	0.16 dp	1.00
NaO_2^- , angular form	2 Na—O—O bend	151.57	<0.01 p	0.13		3 O—K—O sym bend	1193.24	1.00 dp	0.05
	3 Na—O str	414.75	<0.01 dp	0.01	KO_2 , linear form	1 K—O—O bend	90.54	<0.01 p	0.06
	4 Na—O—O asym str	1083.74	1.00 dp	1.00		2 K—O—O bend	121.68	0.09 p	0.06
LiO_2^- , triangular form	1 Na—O—O bend	101.93	0.02 dp	0.01		3 K—O str	347.96	0.09 dp	<0.01
	2 Na—O str	314.62	0.01 dp	<0.01		4 K—O—O asym str	1252.9	1.00 dp	1.00
	3 O—O str	1096.28	1.00 dp	1.00	O_2^-	1 O—O str	1194.17	1.00 dp	none

theoretically the highest energy form as indicated in Table 2. There are no strong theoretical LiO_2^- bands that match the observed 830 cm^{-1} band. The strong band at 1062 cm^{-1} is likely due to the strong KCO_3^- band at 1059 cm^{-1} in Table 1. One cannot completely rule out the possibility that the LiCO_3^- band at 1124 cm^{-1} also contributes. The weak band at 692 cm^{-1} is present in an atmosphere of either O_2 or Ar and is assigned to the Raman vibration of KCO_3^- at 678 cm^{-1} .

Effect of CO_2 . Chen and co-workers⁴ reported the effect of CO_2 on molten Li/K carbonate at 923 K. The Li/K carbonate melt under 1 atm of O_2 produces initial Raman peaks at 620, 832, and 1062 cm^{-1} . As time progresses, a weak band at

982 cm^{-1} is observed. Upon addition of CO_2 to the O_2 atmosphere in the Li/K carbonate melt, the 832 cm^{-1} peak decreases while the peaks at 620 and 982 cm^{-1} grow. The peak at 1062 cm^{-1} remains essentially constant. The authors⁴ suggest that the addition of CO_2 leads to the formation of CO_4^{2-} via eq 2:



This prediction is supported by several Raman bands. The broad peak at 982 cm^{-1} is well represented by the strong Raman vibrations 6–9 (905 – 1037 cm^{-1}) for CO_4^{2-} as given in Table 1. The broad Raman peak at approximately 610 cm^{-1} is

Table 2. B3LYP/(6-311+G(d,p)) Sum of Electronic and Thermal Free Energies at 923 K and 1 atm

species	$G^\circ{}^a$ (au) ^b
O_2^-	-150.452 141
$C_2O_6^{2-}$	-527.812 642
CO_4^{2-}	-338.916 608
CO_4^{4-}	-337.874 808
KCO_4^-	-939.105 058
$LiCO_4^-$	-346.762 904
O^{2-}	-75.052 277
triangular KO_2^-	-750.430 000
linear KO_2^-	-750.437 512
bent KO_2^-	-750.446 818
triangular LiO_2^-	-158.074 821
linear LiO_2^-	-158.002 992
triangular NaO_2^-	-312.808 362
linear NaO_2^-	-312.761 153
bent NaO_2^-	-312.808 730
CO_3^{2-}	-263.813 940
O_2	-150.398 101
CO_3^-	-264.004 287
$(CO_3^{2-})_2$	does not exist
CO_5^{2-}	-414.253 439
CO_2	-188.740 224
CO_4^-	-339.115 387
O_2^{2-}	-150.099 115
KCO_3^-	-864.021 719
$LiCO_3^-$	-271.636 945
$NaCO_3^-$	-426.380 743
H_2O_2	-151.679 163
K^+	-599.835 047
Li^+	-7.349 196
Na^+	-162.158 495
triangular KO_2	-750.488 221
linear KO_2	-750.463 320
triangular LiO_2	-158.074 822
linear LiO_2	-158.041 282
triangular NaO_2	-312.833 169

^aSum of electronic and thermal free energies; calculations done at 923 K and 1 atm. ^b1 au = 627.5095 kcal/mol.

also matched by the theoretical O–C–O bend and stretch vibration at 603 cm⁻¹.

A modification of the above prediction (eq 2) is to include the reaction of CO_4^{2-} with K^+ to form KCO_4^- via eq 3:



The broad peak at 982 cm⁻¹ can be represented by the KCO_4^- bands (Table 1) from 888 to 1122 cm⁻¹. The sum of these bands (weighted) is 964 cm⁻¹. There is also a weaker vibration at 602 cm⁻¹. It is likely that the observed spectrum is due to a combination of these vibrations for CO_4^{2-} and KCO_4^- .

Presence of O_2 . Itoh^{3,5} combined electrochemical analysis with surface-enhanced Raman scattering (SERS) to study the Li/K carbonate eutectic at 923 K and the Li_2CO_3 melt at 1123 K. Raman lines were observed at 800, 1047, and 1080 cm⁻¹ for both melts and at 735 cm⁻¹ for the Li_2CO_3 melt in the presence of O_2 . Their results^{3,5} suggested that oxygen reduction in the Li_2CO_3 melt involved only peroxide ions while oxidation in the Li/K carbonate eutectic involved the peroxide and superoxide species. The observed^{3,5} Raman lines at 800 cm⁻¹ can be assigned to the 768 cm⁻¹ Raman band for the triangular

form of LiO_2 given in Table 1. The linear (higher energy) form of LiO_2^- also has a band at 772 cm⁻¹ that cannot be completely ruled out. In the Li_2CO_3 melt, LiO_2^- has theoretical Raman lines at 949 and 1081 cm⁻¹ (Table 1). In the Li/K eutectic melt, the same lines can be represented by those mentioned above for the Li_2CO_3 melt in addition to the 804 and 1080 cm⁻¹ Raman bands calculated for the triangular and linear versions of KO_2^- .

Energetic Limitations on Raman Assignments. The data given in Table 2 indicate that certain of the theoretically possible forms are more favored than others. The three forms of KO_2^- should exist (gas phase) in the approximate ratio of 85:12:1 for the bent, linear, and triangular forms. The assignment of the strong KO_2^- Raman band at 830 cm⁻¹ with the theoretical vibration at 804 cm⁻¹ is made on the basis of a theoretically strong vibration that matches the experimental result.

The ratio of the linear form of the triangular form of LiO_2^- to the linear form is approximately 1.7×10^8 :1.00. This effectively rules out any contribution from the triangular form of LiO_2^- . The possible forms of NaO_2^- theoretically exist in the ratio approximately 1.10:1.00 for the bent to triangular forms. The higher energy form (vs triangular and bent forms) of linear NaO_2^- formation limits its participation as a contributing species. The triangular forms of KO_2 and LiO_2 exist in ratios of approximately 720:1 and 10⁴:1 to their linear forms, respectively. It is unlikely that the linear forms of KO_2 and LiO_2 contribute extensively to the Raman spectra of either species.

CONCLUSIONS

In general, the various predictions of high temperature species made in previous articles are reasonably accurate once a coordinating monovalent cation is attached to the anion under discussion.

AUTHOR INFORMATION

Corresponding Author

*E-mail: Bob.Carper@wichita.edu.

Notes

The authors declare no competing financial interest.

ACKNOWLEDGMENTS

The background for this work was developed during a Mercator Visiting Professorship (W.R.C.) at RWTH, Aachen, Germany. Partial support from the Air Force Office of Scientific Research to W.R.C. is also gratefully acknowledged.

REFERENCES

- Bates, J. B.; Brooker, M. H.; Quist, A. S.; Boyd, G. E. *J. Phys. Chem.* **1972**, *76*, 1565–1571.
- Chen, L.-J.; Chang, X.; Lin, C.-J.; Huang, C. M. *Electrochim. Acta* **2002**, *47*, 1475–1480.
- Itoh, T.; Abe, K.; Dokko, K.; Mohamedi, J.; Uchida, I.; Kasuya, A. *J. Electrochem. Soc.* **2004**, *151*, A2042–A2046.
- Chen, L.-J.; Lin, C.-J.; Zuo, J.; Song, L.-C.; Huang, C.-M. *J. Phys. Chem. B* **2004**, *108*, 7553–7556.
- Itoh, T.; Maeda, T.; Kasuya, A. *Faraday Discuss.* **2006**, *132*, 95–109.
- Mizuhata, M.; Ohta, T.; Doki, S. *Electrochemistry* **2009**, *77*, 721–724.
- McPhail, S. J. *Adv. Sci. Technol.* **2010**, *72A*, 283–290.
- Zaza, F.; Paoletti, C.; LoProst, R.; Simonetti, E.; Pasqual, M. *Int. J. Hydrogen Energy* **2011**, *36*, 8119–8125.
- Antolini, E. *Appl. Energy* **2011**, *88*, 4274–4293.
- Sanchez, D.; Munoz de Escalona, J. M.; Chacartegui, R.; Munoz, A.; Sanchez, T. *J. Power Sources* **2011**, *196*, 4347–4354.

- (11) Griffiths, T.; Vokovich, V. A. *Nucl. Technol.* **2008**, *163*, 382–400.
- (12) Griffiths, T.; Vokovich, V. A.; Carper, W. R. In *Molten Salts and Ionic Liquids: Never the Twain?*; Gaune-Escard, M., Seddon, K. R., Eds.; Wiley: Hoboken, NJ, 2010; pp 151–167.
- (13) Griffiths, T.; Vokovich, V. A.; Carper, W. R. *Struct. Chem.* **2010**, *21*, 291–297.
- (14) Talaty, E. A.; Raja, S.; Storhaug, V. J.; Dolle, S.; Carper, W. R. *J. Phys. Chem. B* **2004**, *108*, 13177–13184.
- (15) Heimer, N. E.; Del Sesto, R. E.; Meng, Z.; Wilkes, J. S.; Carper, W. R. *J. Mol. Liq.* **2006**, *124*, 84–95.
- (16) Carper, W. R.; Langenwalter, K.; Nooruddin, N. S.; Kullman, M. J.; Gerhard, D.; Wasserscheid, P. *J. Phys. Chem. B* **2009**, *113*, 2031–2041.
- (17) Berg, R. W. *Monatsh. Chem.* **2007**, *135*, 1045–1075.
- (18) Iwata, K.; Okajima, H.; Saha, S.; Hamaguchi, H. *Acc. Chem. Res.* **2007**, *40*, 1174–1181.
- (19) Frisch, M. J.; Trucks, G. W.; Schlegel, H. B.; Scuseria, G. E.; Robb, M. A.; Cheeseman, J. R.; Montgomery, J. A., Jr.; Vreven, T.; Kudin, K. N.; Burant, J. C.; Millam, J. M.; Iyengar, S. S.; Tomasi, J.; Barone, V.; Mennucci, B.; Cossi, M.; Scalmani, G.; Rega, N.; Petersson, G. A.; Nakatsuji, H.; Hada, M.; Ehara, M.; Toyota, K.; Fukuda, R.; Hasegawa, J.; Ishida, M.; Nakajima, T.; Honda, Y.; Kitao, O.; Nakai, H.; Klene, M.; Li, X.; Knox, J. E.; Hratchian, H. P.; Cross, J. B.; Bakken, V.; Adamo, C.; Jaramillo, J.; Gomperts, R.; Stratmann, R. E.; Yazyev, O.; Austin, A. J.; Cammi, R.; Pomelli, C.; Ochterski, J. W.; Ayala, P. Y.; Morokuma, K.; Voth, G. A.; Salvador, P.; Dannenberg, J. J.; Zakrzewski, V. G.; Dapprich, S.; Daniels, A. D.; Strain, M. C.; Farkas, O.; Malick, D. K.; Rabuck, A. D.; Raghavachari, K.; Foresman, J. B.; Ortiz, J. V.; Cui, Q.; Baboul, A. G.; Clifford, S.; Cioslowski, J.; Stefanov, B. B.; Liu, G.; Liashenko, A.; Piskorz, P.; Komaromi, I.; Martin, R. L.; Fox, D. J.; Keith, T.; Al-Laham, M. A.; Peng, C. Y.; Nanayakkara, A.; Challacombe, M.; Gill, P. M. W.; Johnson, B.; Chen, W.; Wong, M. W.; Gonzalez, C.; Pople, J. A. *Gaussian 03*, revision D.02; Gaussian, Inc.: Wallingford, CT, 2004.